SCIENTIFIC REPORTS

OPEN

SUBJECT AREAS:
CANCER METABOLISM
BIOMARKER RESEARCH

Received
2 January 2014

Accepted
2 June 2014

Published
24 June 2014

Correspondence and requests for materials should be addressed to V.P.S. (vsukhatm@bidmc.harvard.edu)

* These authors contributed equally to this work.

Knockdown of Malic Enzyme 2 Suppresses Lung Tumor Growth, Induces Differentiation and Impacts PI3K/AKT Signaling

Jian-Guo Ren[1]*, Pankaj Seth[1]*, Clary B. Clish[2], Pawel K. Lorkiewicz[3,4], Richard M. Higashi[3,4], Andrew N. Lane[3,5], Teresa W.-M. Fan[3,4,5] & Vikas P. Sukhatme[1]

[1]Divisions of Interdisciplinary Medicine and Biotechnology, Hematology-Oncology and Nephrology, Beth Israel Deaconess Medical Center (BIDMC) and Harvard Medical School, 330 Brookline Avenue, Boston, MA 02215, [2]Metabolite Profiling Initiative, The Broad Institute of MIT and Harvard, 7 Cambridge Center, Cambridge, MA 02142, [3]Center for Regulatory and Environmental Analytical Metabolomics, [4]Department of Chemistry, University of Louisville, Louisville, KY 40208, [5]J. G. Brown Cancer Center, University of Louisville, Louisville, KY 40208.

Mitochondrial malic enzyme 2 (ME2) catalyzes the oxidative decarboxylation of malate to yield CO_2 and pyruvate, with concomitant reduction of dinucleotide cofactor NAD^+ or $NADP^+$. We find that ME2 is highly expressed in many solid tumors. In the A549 non-small cell lung cancer (NSCLC) cell line, ME2 depletion inhibits cell proliferation and induces cell death and differentiation, accompanied by increased reactive oxygen species (ROS) and $NADP^+$/NADPH ratio, a drop in ATP, and increased sensitivity to cisplatin. ME2 knockdown impacts phosphoinositide-dependent protein kinase 1 (PDK1) and phosphatase and tensin homolog (PTEN) expression, leading to AKT inhibition. Depletion of ME2 leads to malate accumulation and pyruvate decrease, and exogenous cell permeable dimethyl-malate (DMM) mimics the ME2 knockdown phenotype. Both ME2 knockdown and DMM treatment reduce A549 cell growth *in vivo*. Collectively, our data suggest that ME2 is a potential target for cancer therapy.

Lung cancer is the leading cause of cancer deaths[1] and approaches other than conventional chemotherapy or radiation therapy are needed for prolonging survival of lung cancer patients. Approximately 75% of lung cancer is non small cell lung cancer (NSCLC)[2]. Mutations in *EGFR*, *KRAS*, *LKB1* and *PTEN*, and over-expression of *MYC* have been described[3,4]. A549, a human adenocarcinoma NSCLC cell line[5,6] which is widely used for lung cancer studies[7,8], carries mutations in LKB1[9] and KRAS. Although the gene is intact, the p53 protein is degraded in these cells due to deletion of the p14ARF locus[10]. A549 cells have wild-type genes for epidermal growth factor receptor EGFR, PTEN and MYC.

Malic enzymes catalyze the divalent metal ion (Mn^{2+} or Mg^{2+}) dependent oxidative decarboxylation of malate to yield pyruvate and CO_2, accompanied by the production of NADH or NADPH[11]. Three isoforms have been identified: cytosolic $NADP^+$-dependent (ME1), mitochondrial $NAD(P)^+$-dependent (ME2), and mitochondrial $NADP^+$-dependent malic enzyme (ME3). ME2 responds to elevated amino acids and may supply pyruvate to increase TCA flux when glucose is limiting[12]. ME2 activity increases with progression to neoplasia in a rat tracheal epithelial line[13] with similar findings in Morris hepatomas[14]. The first functional connection between ME2 expression and cancer was recently published: knockdown of ME2 in K562 cells led to erythroid differentiation in this model of chronic myelogenous leukemia[15].

Here, we have investigated the role of ME2 in lung cancer using A549 cells. Knockdown of ME2 induced cell death and differentiation in vitro and impacted the PI3K/AKT/mTOR pathway. Supplementation of cell permeable dimethyl-malate (DMM) mimicked the phenotype caused by ME2 depletion. Moreover, depletion of endogenous ME2 or administration of DMM inhibited tumor growth in vivo. These data suggest that ME2 may be a potential target for lung cancer therapy.

Results

ME2 expression in lung tumor tissues. We hypothesized that ME2 might be overexpressed in clinical tumor samples. In eighty specimens representing 13 types of solid tumors (Purchased from Protein Biotechnologies, CA), ME2 protein was overexpressed in a large number (Table S1, Figure S1). About 90% of lung tumors overexpressed ME2 (Table S2 and Figure S2a and b). We investigated ME2 expression in a human tumor tissue array from US Biomax containing 8 types of solid tumors to assess ME2 expression in cancer versus normal tissue, and found that ME2 in lung cancer significantly higher than normal tissue (Figure S2c and Figure S3). Moreover, we also found that ME2 was overexpressed in several other tumor types (Figure S3). In another separate tissue array containing 100 melanoma samples, we found that ME2 expression is correlated to melanoma disease stage (Figure S4a). Similar data was obtained with primary versus lymph node metastases in melanoma (Figure S4b). These data suggest that ME2 may play a role in cancer broadly and particularly in lung cancer.

ME2 knockdown impairs A549 cells proliferation and reprograms metabolism. In A549 cells, all three constructs showed marked ME2 knockdown (Figure 1a), and knockdown of ME2 inhibited tumor cells proliferation (Figure 1b) and colony formation (Figure 1g). Similar results were obtained in three independent single clones (Figure 1c and d), and one different lung cancer cell line: H1650 (a lung cancer line resistant to TKI inhibition) (Figure 1e and f), as well as MCF-7 cells (a breast cancer line) (Figure S2f and g), WM983B (Figure S2h and i) and WM852 cells (melanoma cell lines) (Figure S2j and k).

To assess whether ME2 knockdown reprograms tumor cell metabolism, we performed stable isotope-resolved metabolomics (SIRM) studies by incubating ME2 knockdown or control cells in uniformly ^{13}C enriched glucose ($^{13}C_6$-Glc) or $^{13}C/^{15}N$ enriched glutamine ($^{13}C_5$, $^{15}N_2$-Gln). ME2 knockdown cells showed a decrease in the $^{13}C_6$-Glc-derived fatty acyl chains (Figure 1h). The m(even) and m(odd $>$ 3) isotopologues represent intact phospholipids in which only the acyl chains are enriched in ^{13}C acetyl moieties and phospholipids where both the fatty acyl chains and the glycerol backbone are enriched in ^{13}C[16] as shown for the most abundant membrane lipids, phosphatidylcholine (PC) (Figure 1h). The decreased synthesis of the membrane lipids is paralleled by reduced protein biosynthesis, as evidenced by decreased consumption of essential amino acids such as Val from the medium (Figure 1i), consistent with diminished cell proliferation.

Survival of ME2 knockdown cells is exquisitely dependent on glucose. Neither control nor ME2 knockdown cells could survive in Hams/F12 medium in the absence of pyruvate, glucose and

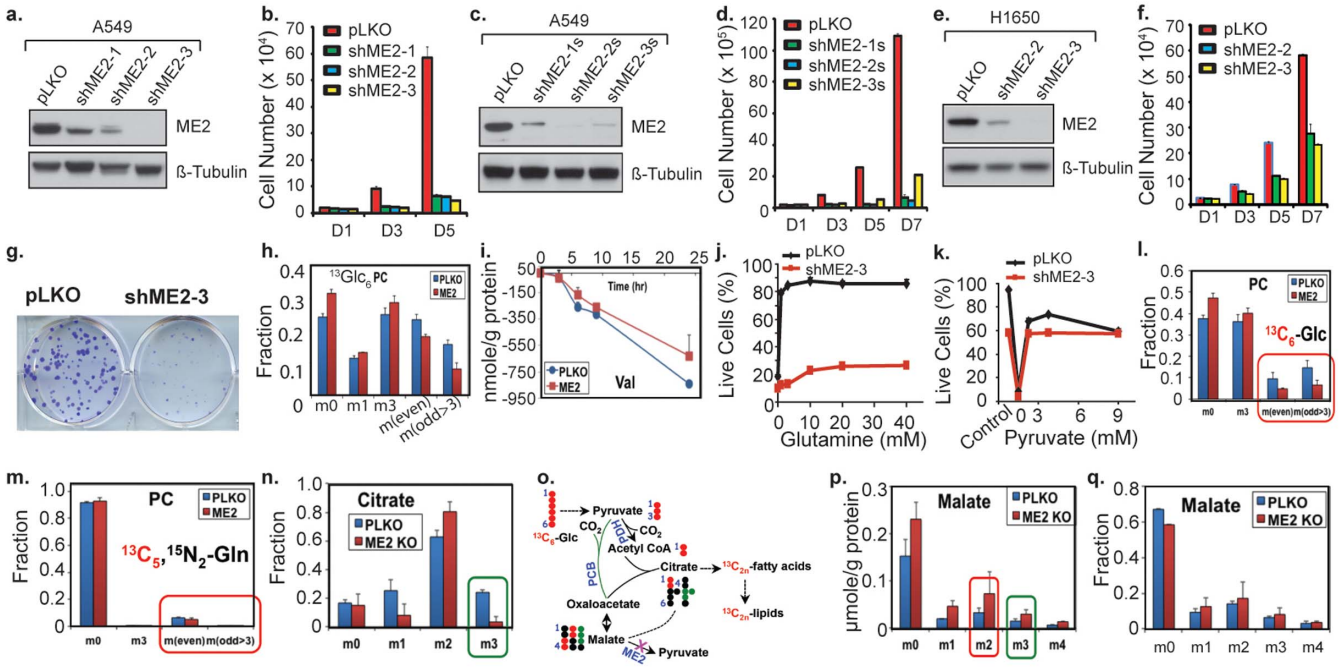

Figure 1 | ME2 depletion inhibits proliferation. (a), Knockdown of ME2 in pools of A549 with three independent ME2 shRNA lentiviruses. The full-length blots are presented in Supplemental Figure S7. (b), Cell proliferation with ME2 knockdown as described in "a". (c), ME2 knockdown in single clones. The full-length blots are presented in Supplemental Figure S8. (d), Cell proliferation of single clones with ME2 knockdown as described in "c". (e), Knockdown ME2 in H1650 cells. The full-length blots are presented in Supplemental Figure S9. (f), Cell proliferation with ME2 knockdown as described in "e". (g), Knockdown of ME2 in A549 inhibits colony formation. (h), Fractional changes in ^{13}C mass isotopologues (differing in the number of ^{13}C atoms) of phosphatidylcholines (PC) in ME2 knockdown cells; m0: all ^{12}C, m3: $^{13}C_3$-PC (^{13}C labeling in glycerol backbone only), m(even): $^{13}C_{even\#}$-PC (^{13}C labeling in fatty acyl chains only), m(odd $>$ 3): $^{13}C_{odd\#>3}$-PC (^{13}C labeling in fatty acyl chains plus glycerol backbone). (i), Time courses of valine consumption, as determined from ^{1}H NMR data. Metabolite data were expressed mean ± SEM, n = 2. (j), The effect of glutamine supplementation on ME2 depletion induced cell death. (k), Pyruvate rescues ME2 knockdown induced cell death. (l) and (m), The effect of ME2 knockdown on de novo synthesis of PC is greater with $^{13}C_6$-Glc than with $^{13}C_5$,1 $^{5}N_2$-Gln as tracer. (n), Inhibition of $^{13}C_3$-citrate synthesis from $^{13}C_6$-Glc by ME2 knockdown. (o), ^{13}C atom-resolved tracing from $^{13}C_6$-Glc through glycolysis, the Krebs cycle without or with input of pyruvate carboxylation, and biosynthesis of fatty acyl chains with even number of ^{13}C ($^{13}C_{2n}$) in lipids via citrate; respectively •,•: ^{13}C atoms from the first turn of Krebs cycle without or with pyruvate carboxylation; solid and dashed arrows: single and multiple-step reactions; single and double-headed arrows: irreversible and reversible reactions; PDH: pyruvate dehydrogenase; PCB: pyruvate carboxylase. (p) and (q), Effects of ME2 knockdown on the levels and fractional distribution of ^{13}C isotopologues of malate; red and green rectangles depict $^{13}C_2$- (m2) and $^{13}C_3$-malate (m3) species as markers of the first turn of the Krebs cycle without and with pyruvate carboxylation input, respectively. Metabolite data were expressed mean ± SEM, n = 2.

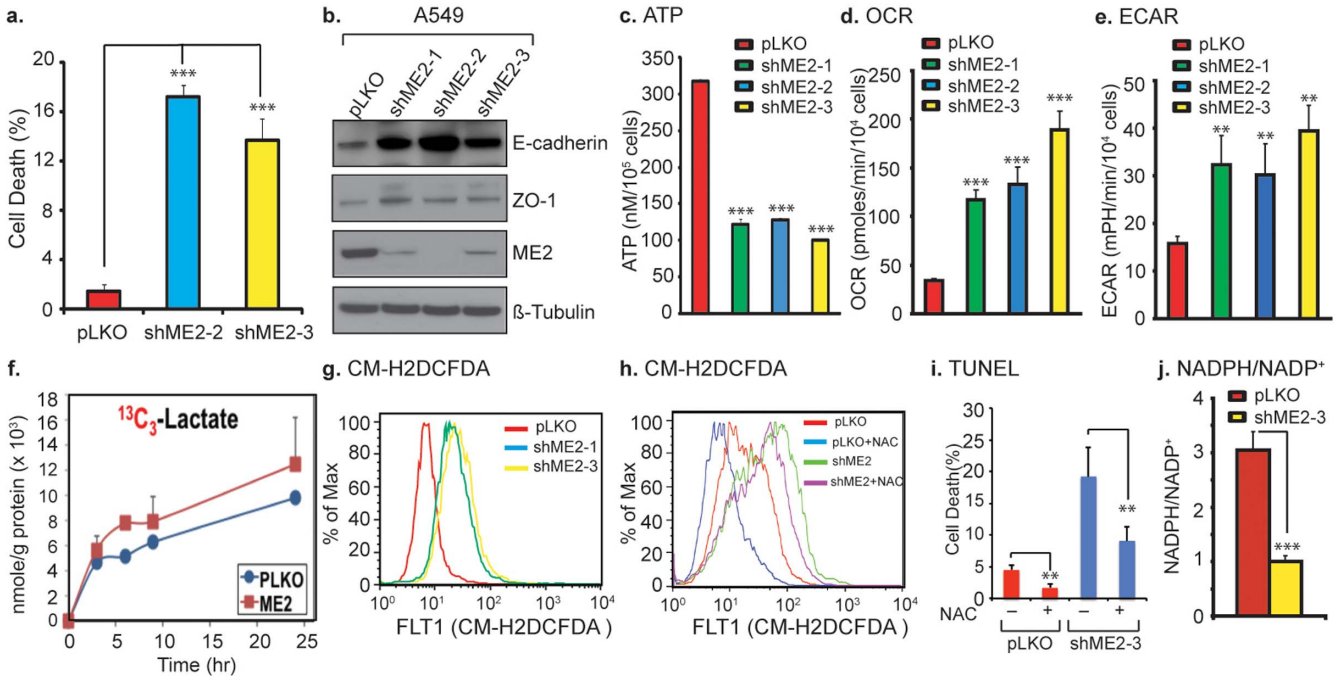

Figure 2 | Knockdown of endogenous ME2 induces A549 cell death and differentiation, and inhibits ATP and NADPH production, while enhancing A549 cells oxygen consumption and ROS production. (a), Depletion of ME2 increases A549 basal cell death. (b), E-cadherin, ZO-1, ME2 and β-tubulin in A549 cells with or without ME2 knockdown were determined by Western blotting. The full-length blots are presented in Supplemental Figure S10. Data are representative of two independent experiments. (c), Depletion of ME2 inhibits ATP production in A549 cells. Data are expressed as mean ± SD, n = 3. (d), Knockdown of ME2 in A549 cells increases O_2 consumption. (e), Knockdown of ME2 in A549 cells increases $[H^+]$ excretion. (f), Increased $^{13}C_3$-lactate excretion induced by ME2 knockdown in A549 cells, as determined by ^1H NMR; data are expressed as mean ± SEM, n = 2. (g), Increased ROS in A549 ME2 knockdown cells detected by flow cytometry using CM-H2DCFDA as probe. Each histogram is representative of three experiments. (h), 5 mM exogenous NAC inhibits ME2 depletion-meditated ROS production. Each histogram is representative of two or three experiments. (i), 5 mM NAC partially rescues ME2 knockdown induced cell death. Control groups without NAC treatment were normalized to 100 and NAC treated groups were compared to its control. Data are expressed as mean ± SD, n = 3. (j), Depletion of ME2 increases NADP/NADPH ratio. Data are expressed as mean ± SD, n = 3.

glutamine (Figure 1j). Supplementation with glutamine rescued control cells more than ME2 knockdown cells. Pyruvate supplementation rescued both ME2 knockdown and control cells (Figure 1k), suggesting that pyruvate produced by ME2 from malate plays a pro-survival role in A549 cells.

Why are ME2 knockdown cells sensitive to glucose deprivation? SIRM studies showed that glucose is the preferred substrate for supporting PC synthesis over glutamine (Figure 1l versus 1m). In addition, the attenuating effect of ME2 knockdown on PC synthesis appears to be greater with $^{13}C_6$-Glc than with $^{13}C_5$, $^{15}N_2$-Gln as tracer (Figure 1l and m) and Gln cannot make glycerol in these cells. Moreover, the glucose-mediated anaplerotic input into the Krebs cycle via pyruvate carboxylation was attenuated in ME2 knockdown cells, as evidenced by the reduced fractional distribution of triply ^{13}C labeled citrate ($^{13}C_3$-citrate or m3 in Figure 1n), which is a unique marker of pyruvate carboxylation (Figure 1o)[17,18]. Citrate is regularly diverted for fatty acid synthesis, which is in turn incorporated into new phospholipids (PLs) (Figure 1o) required for cell proliferation and maintenance. Since citrate replenishment from glucose is already reduced in ME2 knockdown cells, withholding glucose would further compromise their ability to maintain PL homeostasis, thereby curtailing cell growth and survival.

Depletion of ME2 induces cell death and differentiation. Annexin-V assays indicated that ME2 deficient tumor cells had much higher rates of cell death (9.4 to 11.7-fold) than control cells (Figure 2a). On the contrary, depletion of ME2 only slightly increased cell death in normal lung primary epithelial cells (Figure S2d and e). Next, we measured the expression E-cadherin and ZO-1, markers of epithelial cell differentiation, in response to ME2 depletion. As shown in Figure 2b, ME2 knockdown increased E-cadherin and ZO-1 expression in three independent pools. Thus, our data point to two major effects of ME2 deficiency: increased differentiation as exemplified by increases in E-cadherin and ZO-1 expression and a decreased growth rate with cell death as the likely underlying mechanism.

Depletion of ME2 inhibits ATP production, increases oxygen consumption and enhances ROS production. We hypothesized that increased cell death in ME2 deficient cells may reflect a drop in ATP levels since ME2 plays a crucial role in glutamine oxidation via the Krebs cycle[19]. ME2 knockdown led to an approximately 50% drop in ATP level (Figure 2c). A portion of this decrease in ATP levels arose from a decrease in de novo ATP synthesis, as evidenced from stable isotope tracer experiments coupled with FT-ICR-MS analysis, where the total ^{13}C fractional enrichment in ATP from $^{13}C_6$-Glc tracer (at 50% supplement) was lower (42.6% ± 0.4%) for ME2 deficient cells than for control cells (48.9% ± 0.8%).

Next, we asked whether this decrease reflects decreased ATP generation perhaps via a shift from mitochondrial oxidative phosphorylation to fermentative glycolysis. We assessed O_2 consumption and extracellular acidification changes using a Seahorse bioanalyzer. Contrary to our expectations, knockdown of ME2 led to a 3–4 fold increase in oxygen consumption (Figure 2d), suggesting that ME2 depletion might be uncoupling ATP production from oxygen consumption or activating ATP-consuming "futile" cycles with heat production. The latter is unlikely since our data suggests that futile cycles associated with pyruvate cycling in the mitochondrial are

decreased based on decreased pyruvate carboxylation. Moreover, we also observed increased proton extrusion with ME2 knockdown (Figure 2e), consistent with an increased rate of $^{13}C_3$-lactate production and release into the medium using $^{13}C_6$-Glc as a tracer (Figure 2f). Clearly, ME2 depletion leads to dramatic reprogramming of intermediary metabolism.

We hypothesized that ME2 knockdown diminishes anti-oxidant defenses, leading to increased ROS. Compared to empty vector control, we observed increases in basal ROS content in two independent populations of ME2 knockdown cells, as quantified by flow cytometry using CD-H2DCFDA as a fluorescent probe (Figure 2g). Exogenous N-acetylcysteine (NAC) inhibited ME2-mediated ROS production (Figure 2h) and partially rescued cell death (Figure 2i). The NADPH/$NADP^+$ ratio also decreased in ME2 knockdown cells (Figure 2j). These data suggest that anti-oxidant defenses were compromised in ME2 depleted cells.

AKT signaling is down regulated in the ME2 deficient state. Metabolites can signal to canonical molecular pathways[20]. The increased cell death and differentiation in ME2-depleted A549 cells suggested that the PI3K/AKT or the RAS/RAF/MEK/ERK pathway might be inhibited by ME2 knockdown. We first looked at the effects on basal AKT phosphorylation using pAKT T308 and pAKT S473 specific antibodies. Relative to control cells, phosphorylation at both T308 and S473 were markedly diminished in the ME2 deficient cells (Figure 3a and b).

To further confirm the inhibition of AKT activity, we established an inducible shRNA knockdown system. Doxycycline-induced ME2 depletion significantly inhibited AKT activity (Figure 3c and d). ME2 deficiency down regulated phospho-AKT levels in response to EGF stimulation (Figure 3e and f). Those data suggest again that ME2 regulates AKT signaling. Next, we examined molecular events upstream of AKT activation, specifically PDK1 and PTEN. Depletion of ME2 dramatically downregulated PDK1 and p-PDK1 expression (Figure 3e and f), suggesting that ME2 regulates AKT activity via modulation of PDK1 levels. To test whether a parallel pathway impinging on AKT is affected i.e. whether PTEN is involved, we investigated PTEN and p-PTEN expression in both ME2 knockdown and ME2 overexpressing cells. We found that knockdown of ME2 increased PTEN and p-PTEN levels (Figure 3a), whereas overexpression of ME2 in HEK 293 cells enhanced AKT activation and decreased PTEN and p-PTEN expression (Figure 3g and h). These data suggest that ME2 regulate AKT activity via modulation of PTEN and PDK1 expression.

ROS are known activators of AMPK[21], and AMPK can activate PTEN[22]. Since depletion of ME2 leads to an increase in ROS, we probed AMPK expression and activation in ME2 knockdown and ME2 overexpressing cells. Knockdown of ME2 increased AMPK and p-AMPK expression (Figure 3a). These results suggest that down regulation of ME2 increases ROS levels, leading to altered expression levels of AMPK and PTEN, and consequent AKT activation. Importantly, we found no change in pERK with ME2 knockdown or overexpression, supporting the notion that ME2 expression is unlikely to impact RAS activity, since RAS activation is known to increase both ERK phosphorylation and AKT activity.

Supplementation by cell permeable exogenous dimethylmalate (DMM) in A549 cells mimics the ME2 knockdown phenotype. Since a function of ME2 is to convert mitochondrial malate into pyruvate, it was not surprising to observe that knockdown of ME2 leads to malate accumulation (Figure 4a and b) as analyzed by two different methods. This accumulation is mediated through reduced ME2 activity, as evidenced by the accumulation of $^{13}C_2$- and $^{13}C_3$-malate (m2 and m3 in Figure 1p) without changes in their fractional enrichment (Figure 1q), which is consistent with a block in malate catabolism via ME2. $^{13}C_2$- and $^{13}C_3$-malate is presumably derived from $^{13}C_6$-Glc via the sequence of glycolysis and the 1st turn of the Krebs cycle without or with input of pyruvate carboxylation, respectively (Figure 1o)[17,23].

Next, we hypothesized that malate accumulation as a result of reduced ME2 activity was responsible for the phenotype of ME2 knockdown cells. If this were true, exogenous malate might mimic the phenotype-induced by ME2 knockdown. We supplemented the cell culture medium with exogenous cell permeable malate in the form of dimethyl malate (DMM)[24]. Proliferation of A549-pLKO cells was significantly inhibited with 10 and 20 mM DMM supplementation (Figure 4c and d). Also, ME2 depleted cells were more sensitive to DMM treatment (Figure 4c and d). Next, we assayed for cell death using Annexin V expression. DMM treatment induced necrosis in A549 control cells (Figure 4e), and ME2 knockdown cells were more sensitive to DMM treatment. Consistent with enhanced ROS production in ME2 knockdown A549 cells (Figure 2g), exogenous DMM treatment elicited a marked rise in ROS as detected by CM-H2DCFDA (Figure 4f), suggesting that cell death-induced by DMM treatment may be due to increased ROS. Also similar to what was observed for ME2 depletion (Figure 3), 10 and 20 mM exogenous DMM treatment diminished basal AKT and PDK1 activity and increased E-cadherin expression in vitro (Figure 4g and h). These data indicate that supplementation with a cell permeable form of malate closely mimics the phenotype-induced by ME2 knockdown.

Antioxidants N-acetyl-cysteine (NAC) and glutathione (GSH) rescue the phenotype induced by DMM treatment. Since DMM largely mimicked the phenotype mediated by ME2 knockdown, we tested whether inhibiting ROS in DMM-treated cells could rescue the cell death phenotype. We first measured mitochondrial ROS using MitoSOX Red staining. As shown in Figure 5a, when A549 cells were treated with 20 mM DMM for 4 days, cells exhibited intense red fluorescence indicative of superoxide production. DMM treatment in the presence of 20 mM NAC led to complete inhibition of superoxide production in the mitochondria. The DMM-induced ROS production in A549 cells was time-dependent (Figure 5b, left panel) as detected by CM-H2DCFDA fluorescence. Both exogenous NAC and GSH inhibited DMM-induced ROS (Figure 5b middle and right panels). Importantly, NAC and GSH almost completely inhibited cell death induced by 10 mM DMM (Figure 5c). Furthermore, when cells were incubated with DMM and NAC or GSH, there was reversal of differentiation induced by DMM (Figure 5d). NAC or GSH treatment also restored DMM-inhibited basal AKT activity (Figure 5d and f). Collectively, these data show that exogenous NAC or GSH can rescue the phenotype-induced by DMM treatment, suggesting that ROS play a pivotal role in this phenotype.

We asked if DMM selectively kills tumor cells. Perhaps, it selectively increases ROS in tumor versus normal cells. We found this not to be case: DMM increased ROS levels in two normal cell lines (Figure S5a). However, even though DMM triggered ROS increase in both normal and tumor cells, DMM selectively killed tumor cells (Figure S5b), suggesting that anti-oxidant defenses may be more effective in non-tumor cells.

Knockdown of endogenous ME2 suppresses tumor growth *in vivo*. To study the effects of ME2 knockdown on the growth of A549 cells in vivo, we injected vector control and ME2 knockdown clones subcutaneously into nude mice and examined tumor formation and progression. ME2 knockdown cells grew much slower than wild type cells (Figure 6a). Western blotting confirmed knockdown of ME2 in vivo (Figure 6b). We also constructed an shRNA inducible system. In one group (4 mice), each mouse received a control-shRNA inoculation in one flank and an ME2 shRNA clone in the other. After 10 days, both control and ME2 shRNA tumors grew similarly. We then fed the mice 2 mg/ml Dox plus 15% sugar. After 5 weeks, tumor sizes were measured. Similar to data obtained from the constitutive shRNA knockdown, in the inducible system, knockdown of ME2

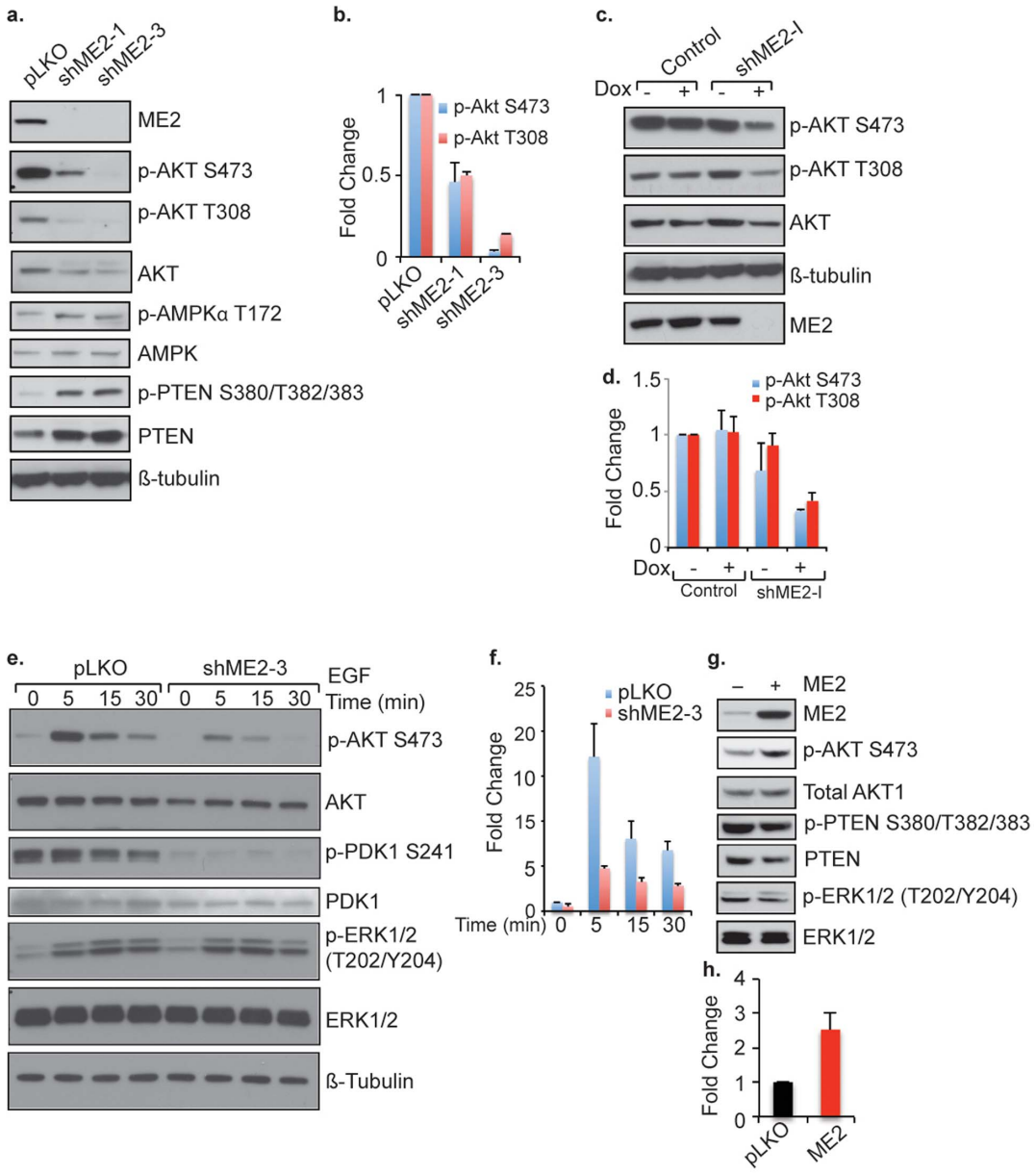

Figure 3 | Knockdown of ME2 inhibits AKT activity in A549 cells. (a), Basal AKT, PTEN and AMPK levels and activation in stable ME2 knockdown cells. The full-length blots are presented in Supplemental Figure S11. (b), Quantitatively analysis p-Akt in "a" by densitometry assay. (c), Inducible shRNA induces ME2 knockdown and inhibits basal AKT activity in A549 cells. The full-length blots are presented in Supplemental Figure S12. (d). Quantitatively analysis p-Akt in "c" by densitometry assay. (e), A549 cell with or without ME2 knockdown were starved for 24 h, and stimulated with 100 ng/ml EGF. The full-length blots are presented in Supplemental Figure S13. (f). Quantitatively analysis p-Akt in "e" by densitometry assay. (g), Overexpression of human ME2 in HEK293 cells enhances AKT activation and decreases PTEN. For this figure, expression levels of ME2, p-AKT473, p-AKT308, AKT, p-PDK1, PDK1, p-ERK1/2, ERK1/2, p-PTEN, PTEN, p-AMPK, AMPK and β-tubulin were determined by Western blotting. The full-length blots are presented in Supplemental Figure S14. (h). Quantitatively analysis p-Akt in "g" by densitometry assay.

also inhibited tumor growth as compared with control shRNA (Figure 6c). Western blot confirmed ME2 knockdown in the inducible system (Figure 6d).

Cisplatin is commonly used to treat NSCLC. It also promotes ROS production. To explore whether knockdown of ME2 may benefit tumor therapy in the context of cisplatin treatment, we investigated the effect of cisplatin on A549 cells with or without ME2 depletion. Deficiency of ME2 in vitro increased the sensitivity of A549 cells in vitro to cisplatin treatment (Figure 6e). We therefore treated A549 xenograft tumors formed from wild type and ME2 knockdown cells with cisplatin. As shown in Figure 6f, ME2 depletion significantly inhibited A549 tumor cell growth in vivo; however, the growth of ME2 knockdown tumors resumed when the tumor size reached about 350 mm^3. Cisplatin treatment could prevent this later tumor growth. ME2 depletion inhibited mucin-1 and vimentin expression, and increased tumor cell expression of E-cadherin and ZO-1 in vivo (Figure 6g). The combination of ME2 depletion and cisplatin showed a particularly striking effect on E-cadherin and mucin-1 expression.

Finally, we tested the anti-tumor activity of DMM in vivo. Administration of 0.5 g/kg DMM significantly inhibited A549 tumor growth (Figure S6a). A combination treatment of DMM and cisplatin showed even more marked effects on tumor growth. We also tested the effect of DMM on tumor growth by directly injecting DMM into A549 tumors: tumors shrank and ulcerated (Figure

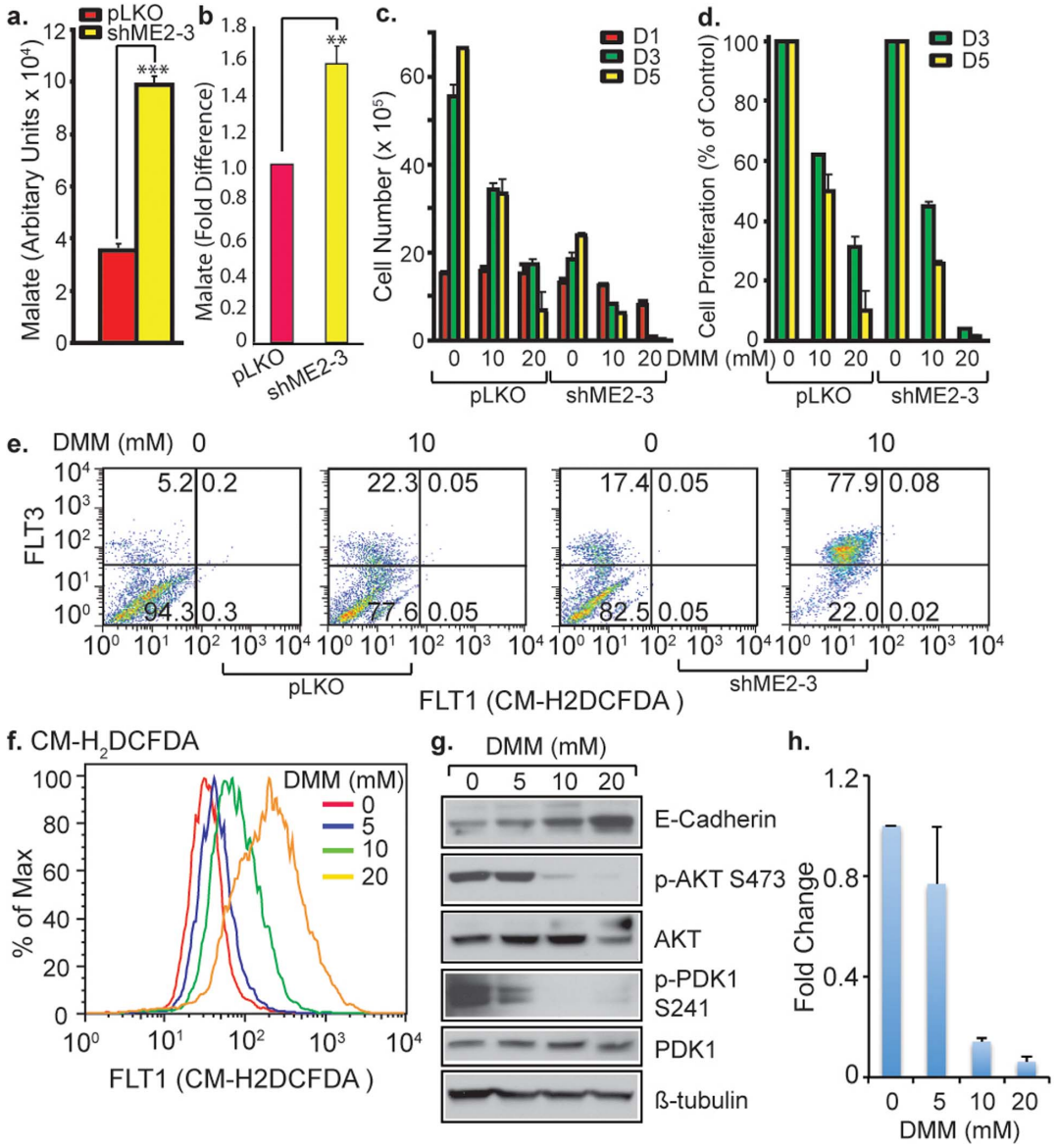

Figure 4 | Supplementation of exogenous cell-permeable DMM mimics the ME2 deficient phenotype. (a), Depletion of ME2 in A549 cells cause malate accumulation analyzed by LC-MS. (b), Malate in ME2 knockdown and control cells were analyzed by malate assay kit. (c), Treatment of A549 control and ME2 knockdown cells with DMM inhibits cell proliferation. (d), ME2 knockdown cells showed more sensitive to exogenous DMM treatment. (e), Exogenous DMM treatment induces A549 control and ME2 knockdown cells undergoing necrosis. (f), Exogenous DMM treatment enhances ROS production. Top: A549 cells treated with 20 mM DMM, and the ROS-induced by DMM were analyzed in different time as indicated; Bottom: ROS-induced by different concentrations of DMM as indicated were analyzed. (g), Exogenous of DMM treatment induces A549 lung cancer cells differentiation, and AKT and PDK1 activity inhibition. The full-length blots are presented in Supplemental Figure S15. (h), Quantitatively analysis p-Akt in "g" by densitometry assay.

S6b). The combination of systemic DMM and cisplatin treatment also induced tumor cell differentiation in vivo, i.e. increased expression of E-cadherin and ZO-1 (Figure S6c).

Discussion

This study extends our previous data on the role of ME2 in leukemic cell differentiation[15] by supporting a role for ME2 in solid tumor growth and differentiation and in lung cancer in particular. It also defines the AKT pathway as a downstream target for ME2 action and points to a role for malate in explaining the ME2 knockdown phenotype.

How does malate accumulation induce cell death and differentiation? Since ME2 depletion causes malate accumulation in A549 cells, the accumulation of malate may enhance mitochondrial ROS production. Indeed, cells treated with a cell permeable form of malate showed inhibition of cell proliferation and increased cell death with a concomitant increase in ROS, similar to the effects observed with ME2 depletion. ROS play a crucial role in regulating cell growth, differentiation and cell death. Cellular ROS levels are finely controlled[25], since high levels of ROS can cause cell death, whereas low levels of ROS can function as a second messenger. ROS can induce cell differentiation in hepatoma[26] and leukemia[27]. ROS production in ME2 knockdown cells increased substantially, and increased ROS production may mediate ME2 knockdown induced cell death and differentiation. In support of this, the anti-oxidant NAC partially rescued the phenotype. Since NAC rescue is presumably mediated via regeneration of GSH, it is possible that the ME2 knockdown cells are unable to utilize GSH for antioxidant defense as evidenced by the

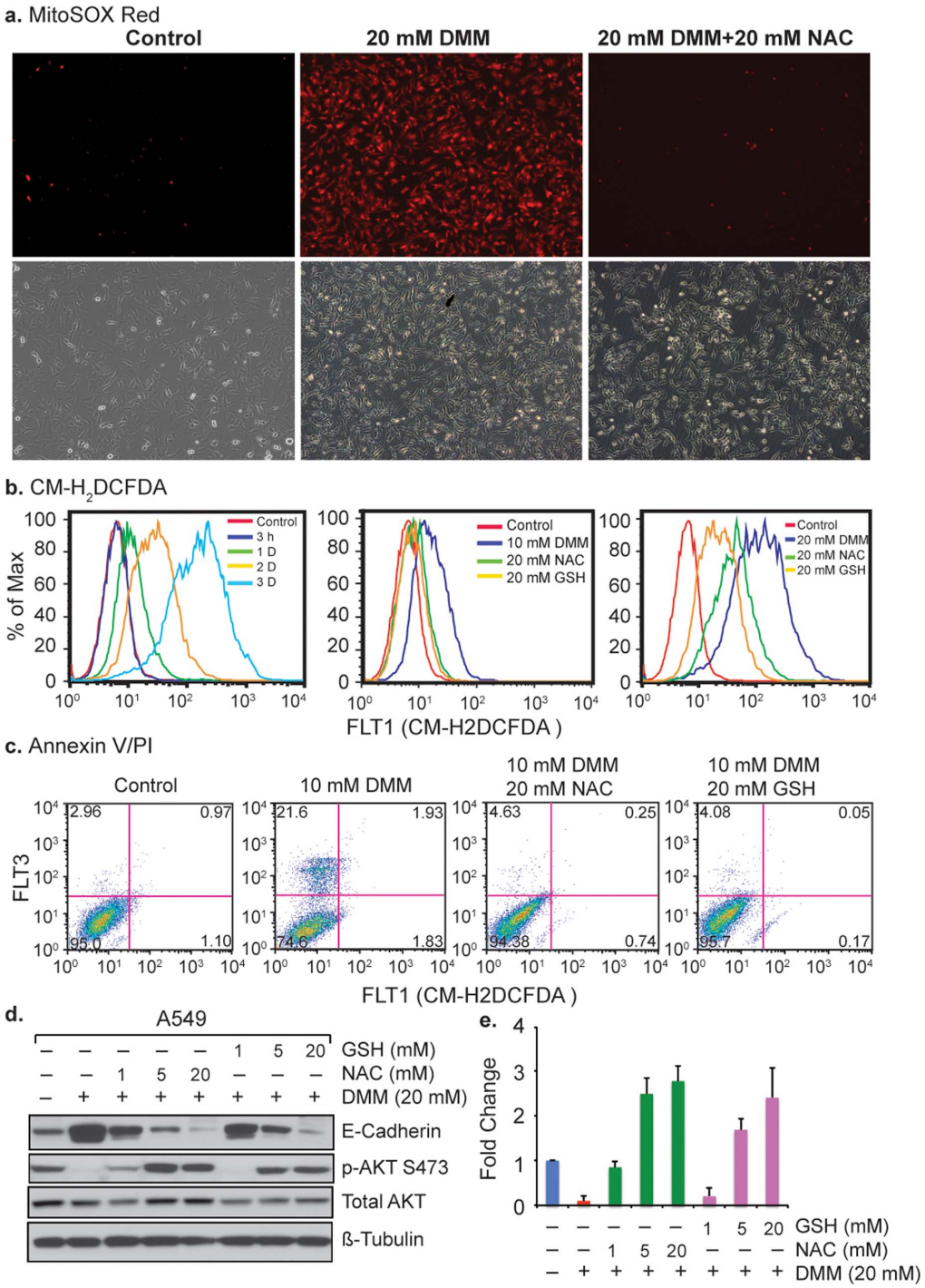

Figure 5 | NAC and GSH rescue exogenous DMM induced phenotype in A549 lung cancers. (a), Accumulation of mitochondrially generated superoxide in A549 cells as detected by MitoSOX (Top: MitoSOX red; Bottom: Phase contrast). Data are representative of two independent experiments. (b), NAC and GSH inhibit the ROS induced by exogenous DMM in A549 cells. ROS in A549 cells detected by flow cytometry using CM-H2DCFDA. Each histogram is representative of three experiments. Left: A549 cells were treated with 10 mM DMM with or without 20 mM NAC or 20 mM GSH. Right: A549 cells were treated with 20 mM DMM with or without 20 mM NAC or 20 mM GSH. (c), NAC or GSH inhibits 10 mM DMM induced cell death. (d), NAC or GSH inhibits DMM induced cell differentiation and rescue the AKT inhibition. The full-length blots are presented in Supplemental Figure S16. (e), Quantitatively analysis p-Akt in "d" by densitometry assay.

fact that the GSH/GSSH ratio did not increase (data not shown), which may also explain why exogenous NAC could not completely rescue the ME2 knockdown phenotype.

How might DMM treatment increase ROS levels? Mitochondrial complex I plays an important role in controlling ROS generation and malate is one of its substrates[28]. Thus, malate accumulation in mitochondria may enhance the TCA cycle, accelerating ROS production. Another way to increase ROS levels is to inhibit antioxidant defenses. $NADPH/NADP^+$ is the principal redox couple involved in intracellular ROS balance. Our data suggests that depletion of ME2 also decreases $NADPH/NADP^+$ ratio (Figure 2j).

ME2 knockdown depletes a source of pyruvate production and this inhibition may also partly contribute to cell growth inhibition. ME2 knockdown cells loss the ability to use glutamine (Figure 1j),

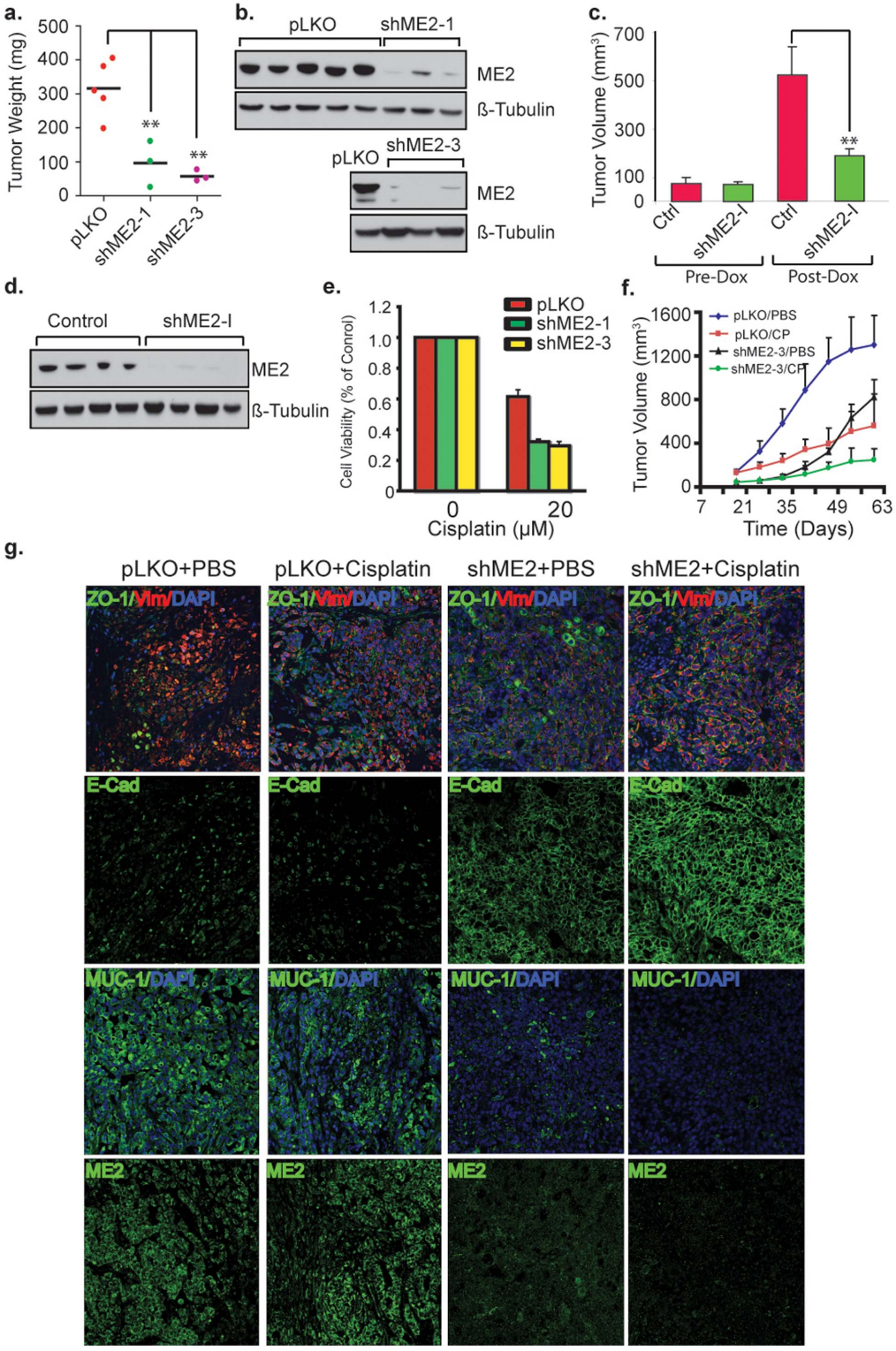

Figure 6 | Stable knockdown of endogenous ME2 levels in A549 cells suppresses tumor formation. (a), A549 cells transfected with ME2 of control shRNA were injected in nude mice separately. Tumor-bearing mice were sacrificed after 6 weeks and the tumors were dissected and weighed. (b), ME2 expression levels from tumor samples (a) were analyzed by Western blotting. The full-length blots are presented in Supplemental Figure S17. (c), A549 cells containing DOX inducible-ME2 specific shRNA or control shRNA cells were subcutaneously implanted into female athymic nude mice. 10 days later, Dox (2 mg/ml) were fed and tumor-bearing mice were sacrificed after 6 weeks and the tumors volume were measured. The tumor volume was calculate using the formula: $V = 0.4AB^2$ (A: Long diameter; B: short diameter). (d), ME2 expression levels from tumor samples (d) were analyzed by Western blotting. The full-length blots are presented in Supplemental Figure S18. (e), Depletion of ME2 renders cells more sensitive to cisplatin treatment. Cells in experiments without cisplatin treatment were normalized to 1 and the cells treated with cisplatin were compared to its control. (f), Stable knockdown of ME2 combined with cisplatin treatment in A549 cells synergistically inhibits tumor size in nude mice. ME2 deficient cells from ME2 specific shRNA or control pLKO cells were subcutaneously implanted into female athymic nude mice. Tumor size was measured and calculated. (g), Depletion of ME2 inhibits mucin-1 and vimentin expression and increase differentiation marker E-cadherin and ZO-1 expression in vivo.

since glutamine supplementation cannot rescue the phenotype. On the contrary, supplementation by exogenous pyruvate can rescue cell death to control levels (Figure 1k). These data indicate that pyruvate production from the action of ME2 is important for cell survival/growth.

In order to obtain energy and essential precursors for the synthesis of macromolecules, tumor mitochondria adapt by overexpressing glutaminase to facilitate the use of glutamate as a fuel. As noted above, high levels of ME2 in tumor cells can enable pyruvate to be produced from malate within the mitochondria to supplement Krebs cycle activity[14,19] and thereby ATP production. Indeed, ME2 is one of the few progression-linked enzymes in Morris hepatomas[14], as is a phosphate-dependent glutaminase[29], suggesting an important role of ME2 in glutamine metabolism in tumors[19]. Asparate production from oxaloacetate may be reduced because pyruvate production from malate is compromised by ME2 knockdown. Since aspartate is a precursor in pyrimidine biosynthesis, depletion of ME2 can also block the synthesis of cellular building blocks.

Our data indicates that knockdown ME2 inhibits ATP, PC (fatty acyl chain), and protein (as evidenced by decreased Val consumption) biosynthesis, which may also explain some of the effects on cell proliferation. This effect on PC appears to be greater with glucose than with Gln as tracer (Figures 1l and 1m). These effects could be mediated via the inhibition of the anaplerotic input from glucose-derived pyruvate into the Krebs cycle via pyruvate carboxylation. This may in part account for the sensitivity of ME2 knockdown to glucose deprivation. Such switch from glutamine to glucose utilization in ME2 knockdown cells reflects the ability of cancer cells to reprogram their metabolism under stress. However, whether depletion of ME2 affects normal cells metabolism is unclear. Normal lung epithelial cells express much less ME2 as compared to A549 cells, and knockdown of ME2 in normal cells only slightly increased cell death, which suggests that ME2 plays a more important role in cell survival in tumor cells than in normal cells.

A549 cells bear a point activating mutation in K-RAS[30]. RAS in turn can activate AKT via a multistep process involving both membrane translocation and phosphorylation. ME2 knockdown dramatically inhibits AKT activity. This result is intriguing in light of the fact AKT is in the cytosol while ME2 localizes to mitochondria. However, recent studies have indicated that AKT activation may be more complex than the canonical view above. In particular, AKT isoforms and PDK1 have been localized to mitochondria[31–33]. Also, cellular redox status may contribute to AKT activation i.e. ROS produced in tumor cells inhibits AKT activity[34,35], which is consistent with our findings. Jiang et al[21] recently found that knockdown of ME2 induced senescence via activation of p53. They found that ROS in ME2 knockdown cells could activate AMPK, which further stabilized p53. In their studies, depletion of ME2 induced senescence and suppressed tumor growth, interestingly even in the $p53^{-/-}$ HCT116 xenograft model. The mechanism for the latter remains uncertain. Our study suggests that in ME2 knockdown cells, AKT is inhibited via two mechanisms: modulation of PTEN and of PDK1 expression. Exogenous DMM mimicked the ME2 knockdown phenotype in A549 cells, increased ROS levels and caused AKT inhibition. Scavenging ROS by NAC rescued DMM mediated AKT inhibition, suggesting that ROS mediate AKT activation. It is worth noting that the effect of ME2 on AKT activity may vary with cell type. In leukemia cells we have previously reported that knockdown of ME2 increases AKT activity[15]. This effect, however, may be due to an effect on hemoglobin synthesis during leukemia cell differentiation and hemoglobin synthesis might stimulate AKT[36].

In conclusion, our data indicate that ME2 plays a crucial role in modulating lung cancer differentiation and growth. Our study also shows that ME2 is overexpressed in a majority of solid tumors. Of note, the p53 protein is degraded in A549 cells due to deletion of the p14ARF locus. Because ARF regulates p53 by binding to MDM2, loss of ARF expression results in hyperactive MDM2 and enhanced degradation of p53[10]. Decreased p53 has been shown to increase ME2 expression, and vice versa[21] . Even if A549 cells retain some functional p53, the amount should be very low because p53 protein is maintained at low steady-state levels even in normal unstressed cells. Therefore, a decreased p53 level will increase ME2 expression. We have also found that inhibition of ME2 suppresses growth of multiple types of cells including lung cancer cells, breast cancer cells and melanoma cells (Figure S2) via the impairment of AKT activity. To the best of our knowledge, this is the first study showing that ME2 is involved in the regulation of AKT signaling transduction pathway. Collectively, our findings highlight ME2 as an attractive target for tumor therapy in a range of tumor types, including those in which p53 is mutated or absent.

Methods

Cell culture and infection. The human lung cancer cell line A549, H1650, normal lung primary epithelial (NLP) cells and breast cancer cell line MCF-7 were obtained from American Type Culture Collection (ATCC) and grown in Hams/F12 Medium (Cellgro, VA), RPMI1640, airway epithelial cell basal medium and DMEM, respectively. All media were supplemented with 10% (v/v) fetal calf serum, 100 units penicillin and 100 μg/ml streptomycin, and grown at 37°C and 5% CO_2. Primary melanoma cell lines (WM983B and WM852) were purchased from Wistar Institute and maintained in melanoma growth medium containing 80% MCDB153, 20% Leibovitz's L-15, 2% FBS, 5 μg/ml Insulin and 1.68 mM $CaCl_2$. A549, H1650, MCF-7, WM983B, WM852 and NLP cells were transduced separately with empty shRNA vector control and three different ME2 shRNA lentiviral particles as previously described[15]. The three ME2 shRNA sequence (sense) used in this study were (Open Biosystem): shME2-1, 5′-CGGCATATTAGTGACAGTGTT-3′; shME2-2, 5′-CCCAGTATGGACACATCTT TA-3′; and shME2-3, 5′-GCACGGCTGAAGA-AGCATAT A-3′. Briefly, A549 cells transduced with lentiviral particles were selected in puromycin (Sigma Aldrich) to generate stable cell lines encoding empty vector shRNA or ME2 shRNA. Hereafter, we named these pools pLKO, shME2-1, shME2-2 and shME2-3, respectively. In order to generate single ME2 knockdown clone, cells from the stable knockdown pools were seeded in a 10-cm plate at 1 : 500 dilution. Individual clones were selected by cloning disc. The single clone corresponding to its parental pools were named pLKO-s, shME2-1s, shME2-2s and shME2-3s, respectively.

Tumor lysate assay and tissue array. Human cancer tissues lysed in RIPA buffer were purchased from Protein Biotechnologies (Protein Biotechnologies, CA) and analyzed for ME2 and β-tubulin expression by Western blotting. The tissue micro arrays used for this study were the human multiple organ cancer tissue micro array (BCN961) from US Biomax, Inc. (Rockville, MD). BCN961 contains 16 types of common organ cancer tissues with matched or unmatched cancer adjacent normal tissue. The array format is 3 cases per type in single core per case. Rabbit anti-ME2 primary antibody (Sigma) was used for ME2 staining. The total positive cell numbers and intensity of anti-ME2 staining were computed and measured by ImageScope from Aperio Scanning System.

Western blotting. A549 cells with and without ME2 knockdown treated were lysed with RIPA buffer (50 mM Tris-HCl, pH 7.4, 150 mM NaCl, 1% NP-40, 0.1% SDS and 0.5% sodium deoxycholate), and equal amount of proteins were resolved by 4%–12% Bis-Tris gels (Invitrogen), as previously described[15].

Proliferation, clonogenic assay and Annexin-V assay. Control and ME2 deficient cell lines were plated in 6-well plate and counted by Coulter counter. For the clonogenic assay, A549 with stably expression ME2 knockdown and control shRNA cells were seeded in a 6-well plate at a density of 200 cells per well. Colonies were fixed with 10% formaldehyde for 5 min and stained with 0.5% crystal violet for 30 min. Cell death was measured by staining with the Nexin reagent using a Nexin kit and counting on the Guava PCA-96 system (Guava Technologies) as per the manufacture's protocol.

Determination of cellular reactive oxygen species (ROS). Intracellular ROS production was measured by staining with CM-H2DCFDA as described earlier[15].

Xenograft model in nude mice. Animal experiments were performed under federal guidelines and approved by the Institutional Animal Care and Use Committee (IACUC) of the Beth Israel Deaconess Medical Center (approval number 0342007). A549 xenografts in nude mice were generated by following the description of Verrax J et al.[37]. Tumor-bearing mice were sacrificed after 6–8 weeks and tumor masses were measured or imaged before excision. Tumor volume were measured and calculate using formula $V = 0.4AB^2$ (A: Long diameter; B: short diameter). ME2 in tumor samples were analyzed by Western Blot.

Intracellular ATP measurements. Intracellular ATP levels in control and ME2 deficient cells were measured by ATP Bioluminescence Assay Kit CLS II (Roche, Germany) according to the manufacturer's instructions as described before[15].

Metabolite profiling. To determine differences in metabolite profiles between ME2-depleted and control cells, metabolite extracts were prepared and then analyzed using liquid chromatography tandem mass spectrometry (LC-MS) as described before[15].

^{13}C-Glucose labeling and ^{13}C metabolite isotopologue distributions analysis. Two separate tracer experiments were performed, each with duplicate samples. For the first experiment, A549 cells were cultured in 10 cm plates for 24 hr in Gln-minus Hams/F12 medium (Sigma) supplemented with 0.2% $^{13}C_6$-Glc (resulting in 50% of glucose as $^{13}C_6$-Glc) or 1 mM $^{13}C_5$, $^{15}N_2$-Gln (Sigma) and 10% dialyzed FBS (10 kDa MWCO, Atlanta Biological). The second experiment was performed similarly with a custom Hams/F12 medium without glucose and Gln (Cellgro, Mediatech) but supplemented with 0.2% $^{13}C_6$-Glc + 1 mM unlabeled Gln (100% of glucose as $^{13}C_6$-Glc) or with 1 mM $^{13}C_5$, $^{15}N_2$-Gln + 0.2% unlabeled Glc. Samples of the medium samples were taken for ^{1}H NMR analysis at 0, 3, 6, 12, and 24 h. Cell metabolism was immediately quenched with cold acetonitrile (−20°C). Both polar and lipid metabolites were extracted in acetonitrile : H_2O : chloroform (2 : 1.5 : 1, v/v) as described previously[18,38]. Metabolites were analyzed by NMR, their MTBSTFA derivatives by gas chromatography-mass spectrometry (GC-MS), and by direct-infusion Fourier transform-ion cyclotron resonance-MS (FT-ICR-MS) as described previously[18,39–41]. Medium metabolites were extracted in cold 10% trichloroacetic acid to precipitate proteins and lyophilized before MTBSTFA derivatization, followed by 1D ^{1}H NMR analysis[17]. Separate aliquots of the medium were deprived with MTBSTFA for GC-MS. The metabolites were identified and quantified using XCalibur software (ThermoFinnigan) for the MS data and MestReNova software (Mestrelab Research) for the NMR data. Results from both NMR and GC-MS measurements were normalized to the total protein weight determined by the BCA method (Pierce).

Statistical analysis. All data are expressed as the mean ± s.d. or SEM and were analyzed using the two-tailed Student t-test or one-way ANOVA. $P < 0.05$ was considered to be significant. *: $P < 0.05$; **: $P < 0.01$; ***:$P < 0.001$. All tests were performed using the Prism software (GraphPad Software, Inc., La Jolla, CA).

1. Zhang, P., Gao, W. Y., Turner, S. & Ducatman, B. S. Gleevec (STI-571) inhibits lung cancer cell growth (A549) and potentiates the cisplatin effect in vitro. *Mol. Cancer* **2**, 1 (2003).
2. Riaz, S. P. *et al.* Trends in incidence of small cell lung cancer and all lung cancer. *Lung Cancer* **75**, 280–284 (2012).
3. Comprehensive genomic characterization of squamous cell lung cancers. *Nature* **489**, 519–525 (2012).
4. Oxnard, G. R., Binder, A. & Janne, P. A. New targetable oncogenes in non-small-cell lung cancer. *J. Clin. Oncol.* **31**, 1097–1104 (2013).
5. Giard, D. J. *et al.* In vitro cultivation of human tumors: establishment of cell lines derived from a series of solid tumors. *J. Natl. Cancer Inst.* **51**, 1417–1423 (1973).
6. Raghu, G., Striker, L., Harlan, J., Gown, A. & Striker, G. Cytoskeletal changes as an early event in hydrogen peroxide-induced cell injury: a study in A549 cells. *Br. J. Exp. Pathol.* **67**, 105–112 (1986).
7. Christofk, H. R., Vander Heiden, M. G., Wu, N., Asara, J. M. & Cantley, L. C. Pyruvate kinase M2 is a phosphotyrosine-binding protein. *Nature* **452**, 181–186 (2008).
8. Rho, J. K. *et al.* Epithelial to mesenchymal transition derived from repeated exposure to gefitinib determines the sensitivity to EGFR inhibitors in A549, a non-small cell lung cancer cell line. *Lung Cancer* **63**, 219–226 (2009).
9. Koivunen, J. P. *et al.* Mutations in the LKB1 tumour suppressor are frequently detected in tumours from Caucasian but not Asian lung cancer patients. *Br. J. Cancer* **99**, 245–252 (2008).
10. Lu, W., Lin, J. & Chen, J. Expression of p14ARF overcomes tumor resistance to p53. *Cancer Res.* **62**, 1305–1310 (2002).
11. Baggetto, L. G. Deviant energetic metabolism of glycolytic cancer cells. *Biochimie* **74**, 959–974 (1992).
12. Guay, C., Madiraju, S. R., Aumais, A., Joly, E. & Prentki, M. A role for ATP-citrate lyase, malic enzyme, and pyruvate/citrate cycling in glucose-induced insulin secretion. *J. Biol. Chem.* **282**, 35657–35665 (2007).
13. Wasilenko, W. J. & Marchok, A. C. Malic enzyme and malate dehydrogenase activities in rat tracheal epithelial cells during the progression of neoplasia. *Cancer Lett.* **28**, 35–42 (1985).
14. Sauer, L. A., Dauchy, R. T., Nagel, W. O. & Morris, H. P. Mitochondrial malic enzymes. Mitochondrial NAD(P)+-dependent malic enzyme activity and malate-dependent pyruvate formation are progression-linked in Morris hepatomas. *J. Biol. Chem.* **255**, 3844–3848 (1980).
15. Ren, J. G., Seth, P., Everett, P., Clish, C. B. & Sukhatme, V. P. Induction of erythroid differentiation in human erythroleukemia cells by depletion of malic enzyme 2. *PLoS One* **5**, doi:10.1371/journal.pone.0012520 (2010).
16. Lane, A. N., Fan, T. W., Xie, Z., Moseley, H. N. & Higashi, R. M. Isotopomer analysis of lipid biosynthesis by high resolution mass spectrometry and NMR. *Anal. Chim. Acta* **651**, 201–208 (2009).
17. Fan, T. W.-M. *et al.* Stable Isotope-Resolved Metabolomic Analysis of Lithium Effects on Glial-Neuronal Metabolism and Interactions. *Metabolomics* **6**, 165–179 (2010).
18. Le, A. *et al.* Glucose-Independent Glutamine Metabolism via TCA Cycling for Proliferation and Survival in B Cells. *Cell Metab.* **15**, 110–121 (2012).
19. Moreadith, R. W. & Lehninger, A. L. The pathways of glutamate and glutamine oxidation by tumor cell mitochondria. Role of mitochondrial NAD(P)+-dependent malic enzyme. *J. Biol. Chem.* **259**, 6215–6221 (1984).
20. Hanai, J. *et al.* Inhibition of lung cancer growth: ATP citrate lyase knockdown and statin treatment leads to dual blockade of mitogen-activated protein kinase (MAPK) and phosphatidylinositol-3-kinase (PI3K)/AKT pathways. *J. Cell Physiol.* **227**, 1709–1720 (2012).
21. Jiang, P., Du, W., Mancuso, A., Wellen, K. E. & Yang, X. Reciprocal regulation of p53 and malic enzymes modulates metabolism and senescence. *Nature* **493**, 689–693 (2013).
22. Kim, S. A. & Choi, H. C. Metformin inhibits inflammatory response via AMPK-PTEN pathway in vascular smooth muscle cells. *Biochem. Biophys. Res. Commun.* **425**, 866–872 (2012).
23. Fan, T. *et al.* Rhabdomyosarcoma cells show an energy producing anabolic metabolic phenotype compared with primary myocytes. *Mol. Cancer* **7**, 79 (2008).
24. Heart, E. *et al.* Role for malic enzyme, pyruvate carboxylation, and mitochondrial malate import in glucose-stimulated insulin secretion. *Am. J. Physiol. Endocrinol. Metab.* **296**, E1354–1362 (2009).
25. Aon, M. A., Cortassa, S. & O'Rourke, B. Redox-optimized ROS balance: a unifying hypothesis. *Biochim. Biophys. Acta* **1797**, 865–877 (2010).
26. Ren, J. G., Zheng, R. L., Shi, Y. M., Gong, B. & Li, J. F. Apoptosis, redifferentiation and arresting proliferation simultaneously triggered by oxidative stress in human hepatoma cells. *Cell Biol. Int.* **22**, 41–49 (1998).
27. Nagy, K., Pasti, G., Bene, L. & Nagy, I. Involvement of Fenton reaction products in differentiation induction of K562 human leukemia cells. *Leuk Res.* **19**, 203–212 (1995).
28. Selivanov, V. A. *et al.* Reactive oxygen species production by forward and reverse electron fluxes in the mitochondrial respiratory chain. *PLoS Comput. Biol.* **7**, e1001115 (2011).
29. Linder-Horowitz, M., Knox, W. E. & Morris, H. P. Glutaminase activities and growth rates of rat hepatomas. *Cancer Res.* **29**, 1195–1199 (1969).
30. Okudela, K. *et al.* K-ras gene mutation enhances motility of immortalized airway cells and lung adenocarcinoma cells via Akt activation: possible contribution to non-invasive expansion of lung adenocarcinoma. *Am. J. Pathol.* **164**, 91–100 (2004).
31. Antico Arciuch, V. G. *et al.* Akt1 intramitochondrial cycling is a crucial step in the redox modulation of cell cycle progression. *PLoS One* **4**, e7523 (2009).
32. Barksdale, K. A. & Bijur, G. N. The basal flux of Akt in the mitochondria is mediated by heat shock protein 90. *J. Neurochem.* **108**, 1289–1299 (2009).
33. Su, C. C., Yang, J. Y., Leu, H. B., Chen, Y. & Wang, P. H. Mitochondrial Akt-regulated mitochondrial apoptosis signaling in cardiac muscle cells. *Am. J. Physiol. Heart Circ. Physiol.* **302**, H716–723 (2012).
34. Kim, S. Y., Bae, S., Choi, K. H. & An, S. Hydrogen peroxide controls Akt activity via ubiquitination/degradation pathways. *Oncol. Rep.* **26**, 1561–1566 (2011).
35. Mawatari, K. *et al.* Reactive oxygen species induced by diamide inhibit insulin-induced ATP-sensitive potassium channel activation in cultured vascular smooth muscle cells. *Asia Pac. J. Clin. Nutr.* **17 Suppl 1**, 162–166 (2008).
36. Ogasawara, N. *et al.* Hemoglobin induces the expression of indoleamine 2,3-dioxygenase in dendritic cells through the activation of PI3K, PKC, and NF-kappaB and the generation of reactive oxygen species. *J. Cell. Biochem.* **108**, 716–725 (2009).
37. Verrax, J., Stockis, J., Tison, A., Taper, H. S. & Calderon, P. B. Oxidative stress by ascorbate/menadione association kills K562 human chronic myelogenous leukaemia cells and inhibits its tumour growth in nude mice. *Biochem. Pharmacol.* **72**, 671–680 (2006).
38. Fan, T. W.-M. in *The Handbook of Metabolomics: Pathway and Flux Analysis, Methods in Pharmacology and Toxicology. DOI 10.1007/978-1-61779-618-0_11* Vol. 17 (eds Fan. T. W.-M., Lane. A. N. & Higashi. R. M.) in press (Springer Science, 2012).
39. Lorkiewicz, P., Higashi, R. M., Lane, A. N. & Fan, T. W. High information throughput analysis of nucleotides and their isotopically enriched isotopologues by direct-infusion FTICR-MS. *Metabolomics* **8**, 930–939 (2012).
40. Lane, A. N., Fan, T. W., Xie, Z., Moseley, H. N. & Higashi, R. M. Isotopomer analysis of lipid biosynthesis by high resolution mass spectrometry and NMR. *Anal. Chim. Acta.* **651**, 201–208 (2009).
41. Fan, T., Bandura, L., Higashi, R. & Lane, A. Metabolomics-edited transcriptomics analysis of Se anticancer action in human lung cancer cells. *Metabolomics* **1**, 325–339 (2005).

Acknowledgments

This work was supported by seed funds from BIDMC to VPS, and an NIDDK training grant to VPS (NIH T32 DK007199) that was used to support JGR. Some data was generated using support from a subaward to VPS from NCI-SAIC-Fredericks (S080221 TO10) and NIH

5R01CA15233 to PS. The funding agencies had no role in study design, data collection and analysis, decision to publish, or preparation of the manuscript.

Author contributions

J.G.R., P.S., A.N.L., T.W.M.F. and V.P.S. designed the experiments. J.G.R., P.S., C.B.C., P.K.L. and R.M.H. carried out the experiments and calculations. J.G.R., A.N.L., T.W.-M.F. and V.P.S. wrote the main manuscript text and J.G.R. prepared all of the figures. All authors reviewed the manuscript.

Additional information

Supplementary information accompanies this paper at http://www.nature.com/scientificreports

Competing financial interests: The authors declare no competing financial interests.

How to cite this article: Ren, J.-G. *et al*. Knockdown of Malic Enzyme 2 Suppresses Lung Tumor Growth, Induces Differentiation and Impacts PI3K/AKT Signaling. *Sci. Rep.* **4**, 5414; DOI:10.1038/srep05414 (2014).